Computational Modeling of *ansa*-Zirconocene Amide Complexes

Adam R. Dunn,[†] Lucas E. Sweet,[†] Dawn C. Wiser,*[,†] Matthew D. LoCoco,[‡] and Richard F. Jordan*[,‡]

Department of Chemistry, Lake Forest College, 555 N. Sheridan Road, Lake Forest, Illinois 60045, and Department of Chemistry, The University of Chicago, 5735 South Ellis Avenue, Chicago, Illinois 60637

Received June 9, 2004

The structures and relative energies of *ansa*-zirconocene bis-amide complexes were studied by DFT computations. X-ray crystal structures and experimental trends in $\Delta E_{rac-meso}$ values for a series of zirconocenes with terminal and chelated bis-amide ligands were reproduced with reasonable accuracy by B3LYP/LANL2DZ//B3LYP/LANL2MB. In the absence of overriding steric interactions, the most stable conformation of Zr{PhN$(CH_2)_3$NPh} rings in zirconocenes is the twist conformation. For $(C_5H_5)_2$Zr{PhN$(CH_2)_3$NPh} (**5**), the twist conformer is 2.7 kcal/mol more stable than the chair and 3.6 kcal/mol more stable than the boat. *rac*-(MBSBI)Zr{PhN$(CH_2)_3$NPh} (*rac*-**3**; MBSBI = Me_2Si(2-Me-4,5-benzindenyl)$_2$) is 5.7 kcal/mol more stable than the *meso* isomer because the latter species must undergo a combination of distortions to accommodate the favored twist conformation of the Zr{PhN-$(CH_2)_3$NPh} ring. These distortions include a significant η^3-slip and an exaggerated angle between the C6 and C5 ring planes for one benzindenyl ligand and a subtle flattening of the Zr{PhN$(CH_2)_3$NPh} ring. In contrast, *rac*-(MBSBI)Zr{PhN$(CH_2)_2$NPh} (*rac*-**7**) is only 2.4 kcal/mol more stable than the *meso* isomer. In this case, the Zr{PhN$(CH_2)_2$NPh} ring adopts an envelope conformation in which one N-*Ph* ring lies in the N−Zr−N plane and steric interactions on the crowded side of the *meso* metallocene unit are minimized. These results provide insight into the origin of *rac/meso* selectivity in chelate-controlled syntheses of *ansa*-zirconocenes based on the reaction of Zr bis-amide compounds with lithium *ansa*-bis-indenyl and cyclopentadienyl reagents.

Introduction

The application of structurally complex *ansa*-metallocenes as stereoselective catalysts has been studied extensively.[1] This field would be advanced significantly by the development of efficient and predictable syntheses of the racemic diastereomers of *ansa*-zirconocenes. Jordan et al. recently reported a highly selective, "chelate-controlled" synthesis of *rac-ansa*-bis(indenyl) zirconocenes, which is based on the reaction of lithium *ansa*-bis(indenyl) salts with the chelated bis-amide compound Zr{PhN$(CH_2)_3$NPh}$Cl_2(THF)_2$ (**1**) and is shown in Scheme 1.[2] This procedure works well for *rac*-(SBI)-Zr{PhN$(CH_2)_3$NPh} (*rac*-**2**) and a variety of substituted derivatives thereof, such as *rac*-(MBSBI)Zr{PhN$(CH_2)_3$-NPh} (*rac*-**3**), as well as *rac*-(EBI)Zr{PhN$(CH_2)_3$NPh} (*rac*-**4**).[3] *rac*-(XBI)Zr{PhN$(CH_2)_3$NPh} species are stereospecifically converted to the corresponding *rac*-(XBI)-$ZrCl_2$ compounds, which are typical catalyst precursors, by reaction with HCl.[2,3]

Scheme 1

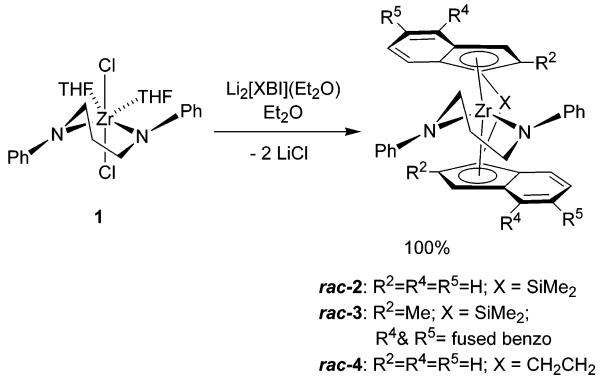

***rac*-2**: R^2=R^4=R^5=H; X = $SiMe_2$
***rac*-3**: R^2=Me; X = $SiMe_2$; R^4& R^5= fused benzo
***rac*-4**: R^2=R^4=R^5=H; X = CH_2CH_2

Jordan et al. proposed the simple model in Scheme 2 to explain the high stereoselectivity in Scheme 1.[2] The Zr{PhN$(CH_2)_3$NPh} rings in **1** and the representative metallocenes *rac*-**2**, *rac*-**3**, and Cp_2Zr{PhN$(CH_2)_3$NPh} (**5**) adopt twist conformations, as shown in Schemes 1 and 2. The twist conformation places the N-*Ph* groups

[†] Lake Forest College.
[‡] The University of Chicago.

(1) (a) Brintzinger, H. H.; Fischer, D.; Mülhaupt, R.; Rieger, B.; Waymouth, R. M. *Angew. Chem., Int. Ed. Engl.* **1995**, *34*, 1143. (b) Resconi, L.; Cavallo, L.; Fait, A.; Piemontesi, F. *Chem. Rev.* **2000**, *100*, 1253. (c) Hoveyda, A. H.; Morken, J. P. *Angew. Chem., Int. Ed. Engl.* **1996**, *35*, 1262. (d) Halterman, R. L. In *Synthesis of Chiral Titanocene and Zirconocene Dichlorides*; Togni, A., Halterman, R. L., Eds.; Metallocenes: Synthesis, Reactivity, Applications; Wiley-VCH: Weinheim, 1998; Vol. 1, Chapter 8.

(2) (a) Zhang, X.; Zhu, Q.; Guzei, I. A.; Jordan, R. F. *J. Am. Chem. Soc.* **2000**, *122*, 8093. (b) LoCoco, M. D.; Jordan, R. F. *Organometallics* **2003**, *22*, 5498.

(3) Abbreviations: SBI = Me_2Si(indenyl)$_2$; MBSBI = Me_2Si(2-Me-4,5-benzindenyl)$_2$; EBI = 1,2-ethylenebis(indenyl); Ind = indenyl; Cent = centroid; X = generic bridge; XBI = generic *ansa*-bis-indenyl.

10.1021/om049576d CCC: $27.50
Publication on Web 10/20/2004

Scheme 2

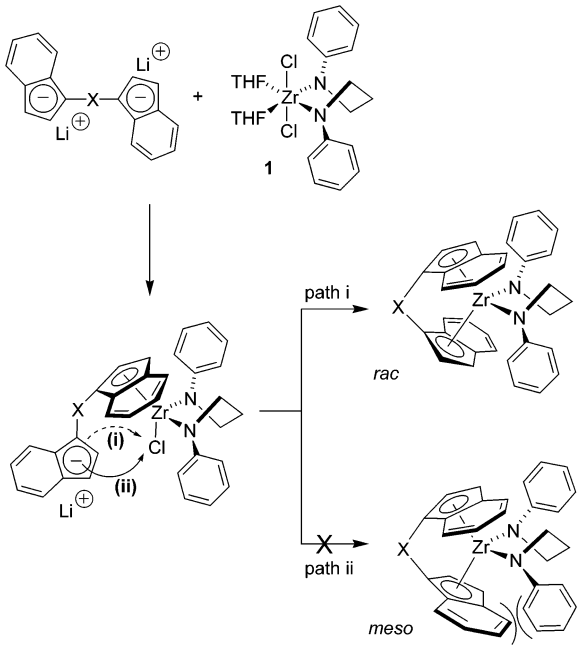

on opposite sides above and below the N−Zr−N plane, which complements the *rac*-metallocene structure and sterically disfavors the *meso* isomer. It is presumed that the metallocene is formed by two successive, irreversible ligand substitution steps, in which the two indenyl groups displace the chloride and THF ligands. The diastereoselectivity is set in the second indenyl addition step. The detailed mechanism of these ligand substitutions is unknown and may be complicated by ion-pairing, solvation, and other factors.[4] However, we postulate that the bridge (X) must be close to the "back" position and the Zr{PhN$(CH_2)_3$NPh} chelate must be in the favored twist conformation in the stereodetermining transition state for the second indenyl addition, as required in the rigid *ansa*-metallocene product. As the second indenyl is added, N-*Ph*/indenyl steric interactions block path (ii), which leads to the *meso* product, and the *rac* product forms by path (i).[5] Significant distortion of the twist chelate conformation and/or the *ansa*-metallocene unit would be required to form the *meso* isomer.

Studies of the reactions of lithium *ansa*-bis(indenyl) salts with other Zr amide complexes provide support for the proposed role of the Zr{PhN$(CH_2)_3$NPh} ring conformation in controlling the stereoselectivity in Scheme 1.[2] For example, the reaction of [Zr{PhN$(CH_2)_2$NPh}-Cl_2(THF)]$_2$ (**6**) with Li_2[MBSBI] yields a 2:1 mixture of *rac*- and *meso*-(MBSBI)Zr{PhN$(CH_2)_2$NPh} (*rac*- and *meso*-**7**) as shown in Scheme 3. The Zr{PhN$(CH_2)_2$NPh} rings in **6** and *rac*- and *meso*-**7** have envelope conformations that place one of the N-*Ph* rings in the N−Zr−N plane. Thus, in this case the Zr-bis-amide chelate ring can accommodate both the *rac* and *meso* zirconocenes

Scheme 3

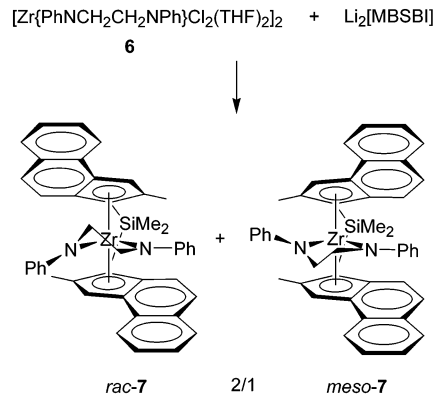

and presumably the transition states leading thereto, and both isomers are formed.

In recent years, computational investigations have contributed to the understanding of organometallic reactions by modeling proposed intermediates and high-energy structures.[6] These studies have been particularly useful with regard to questions involving stereocontrol. Here we describe computational studies of zirconocene amide complexes using low-level density functional theory (DFT). The objectives of this work were (i) to implement and validate an efficient computational procedure for predicting the structures and relative energies of zirconocene amide complexes, (ii) to investigate the structures and energies of *meso*-(XBI)Zr{PhN-$(CH_2)_3$NPh} species to determine if and why they are less stable than the *rac* isomers, (iii) to probe the conformational properties of Zr{PhN$(CH_2)_3$NPh} rings to test the hypothesis that the twist conformation is generally favored in such systems, and (iv) to use the results of these investigations in a predictive manner to design new syntheses.

Computational Details

Geometry Optimization. For each zirconocene, a conformational search was performed with the molecular mechanics Reaction Force Field (RFF)[7] using conjugate velocity molecular dynamics.[8] The lowest energy structure from this search was optimized using RFF. For zirconocenes containing a chelated bis-amide ligand, the starting structures for the RFF conformational search included all reasonable conformations of the chelate ring (e.g., chair, boat, twist, and envelope for a six-membered ring). The RFF was found to overestimate the N−Zr−N angle for chelated bis-amide complexes by as much at 11° compared with X-ray crystal structure data, and therefore the RFF N−Zr−N angle was constrained in these cases.[9] For zirconocenes containing two monodentate amide ligands, no N−Zr−N constraints were necessary to accurately reproduce the N−Zr−N angle.

The RFF optimized geometries were used as starting points for geometry optimizations using DFT. The DFT optimizations used Becke's three-parameter hybrid functional (B3)[10] coupled with the Lee, Yang, and Parr correlation functional (LYP)[11] and the LANL2MB basis set (B3LYP/LANL2MB). The

(4) Wiesenfeldt, H.; Reinmuth, A.; Barsties, E.; Evertz, K.; Brintzinger H. H. *J. Organomet. Chem.* **1989**, *369*, 359.

(5) In contrast, metallocene syntheses using Ti binaphtholate or Zr biphenolate compounds that adopt twist conformations gave low yields,[a] or *rac*/*meso* mixtures that were isomerized to *rac* products using TEMPO.[b] (a) Erikson, M. S.; Fronczek, F. R.; McLaughlin, M. L. *J. Organomet. Chem.* **1991**, *415,* 75. (b) Damrau, H.-R.; Royo, E.; Obert, S.; Schaper, F.; Weeber, A.; Brintzinger, H.-H. *Organometallics* **2001**, *20*, 5258.

(6) (a) Niu, S.; Hall, M. B**.** *Chem. Rev.* **2000**, *100*, 3535. (b) Rappé, A. K.; Skiff, W. M.; Casewit, C. J. *Chem. Rev*. **2000**, *100*, 1435−1456.

(7) (a) Rappé, A. K.; Pietsch, M. A.; Wiser, D. C.; Hart, J. R.; Bormann-Rochotte, L. M.; Skiff, W. M. *Mol. Eng*. **1997**, *7*, 385. (b) Wiser, D. C. Ph.D. Thesis, Colorado State University, Fort Collins, CO, 1995. (c) Bormann-Rochotte, L. M. Ph.D. Thesis, Colorado State University, Fort Collins, CO, 1998.

(8) Rappé, A. K.; Casewit, C. J. Calleo Scientific Software; 1998.

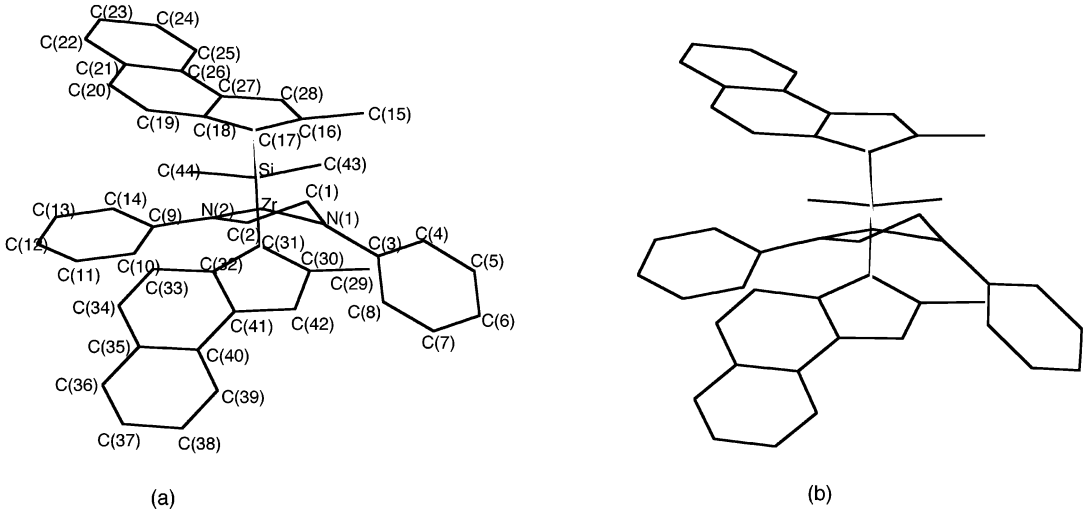

Figure 1. (a) Calculated (B3LYP/LANL2MB) structure for *meso*-(MBSBI)Zr{PhN(CH_2)$_2$NPh} (*meso*-**7**). H atoms are omitted. Bond distances (Å): Zr−N(1) 2.06, Zr−N(2) 2.10, Zr−Centroid(1) 2.46, Zr−Centroid(2) 2.35. Bond angles (deg): N(1)−Zr−N(2) 82.94, Centroid(1)−Zr−Centroid(2) 119.4. Torsion angles (deg): N(2)−Zr−N(1)−C93) 139.5, C(9)−N(2)−Zr−N(1) −163.3. ∑ angles around N (deg): N(1) 359.4, N(2) 359.5. (b) X-ray structure of *meso*-**7**.[2a]

LANL2MB basis set uses the minimal STO-3G basis set for C, H, N, O, and Si and the Hay and Wadt effective core potentials for Zr.[12] The N−Zr−N angle was not constrained in the DFT calculations. Frequency calculations at B3LYP/LANL2MB were performed on the DFT optimized geometries to confirm that the structures were true minima. All DFT calculations were performed using Gaussian 98.[13]

Energies. All reported energies were obtained from DFT single-point energy (SPE) calculations using B3LYP with the LANL2DZ basis set. The LANL2DZ basis set uses a Dunning/Huzinaga full double-ξ basis set on C, H, N, O, and Si[14] and the Hay and Wadt effective core potentials at Zr. These SPE calculations were performed on the B3LYP/LANL2MB optimized geometries (B3LYP/LANL2DZ//B3LYP/LANL2MB). Because geometry optimizations were not performed with the LANL2DZ basis set, the reported energies do not include thermal corrections to enthalpy, entropy, or zero-point effects.[15]

Results

Validation of Methodology: Structures. Calculated (B3LYP/LANL2MB) structures were compared to crystallographically determined structures for five representative *ansa*-zirconocene amide complexes: *rac*-**7**,[2a] *meso*-**7**,[2a] *rac*-**3**,[2a,16] *rac*-(SBI)Zr(NMe_2)$_2$ (*rac*-**8**),[17] and *rac*-(EBI)Zr(NMe_2)$_2$ (*rac*-**9**).[18] The agreement between calculated and X-ray structures was assessed by comparison of four key structural features: the chelate ring conformation, selected bond lengths and angles, trends in Zr−$C_{indenyl}$ bond lengths, and the angle between the planes of the C6 and C5 rings of the indenyl ligands.

Chelate Ring Conformation. The calculated structures of *meso*-**7** and *rac*-**7** are shown in Figures 1 and 2. In both cases, the Zr{PhN(CH_2)$_2$NPh} rings are predicted to adopt envelope conformations that are very similar to those found in the X-ray structures. In both cases, one N-*Ph* group lies nearly in the N−Zr−N plane while the other N-*Ph* group is directed significantly out of the N−Zr−N plane. For *rac*-**3**, the Zr{PhN(CH_2)$_3$NPh} chelate ring is predicted to adopt a twist conformation which places the two N-*Ph* groups on opposite sides of the N−Zr−N plane, in agreement with X-ray data (Figure 3). The conformations of the Zr{PhN(CH_2)$_n$NPh} (n = 2, 3) rings in these structures can be defined by the deviations of the ring atoms from the N−Zr−N plane. As summarized in Table 1, good agreement between the calculated and X-ray-determined ring conformations is observed.

Bond Lengths and Angles. The calculated bond lengths and angles agree reasonably well with X-ray data. Table 2 compares the values for key distances and angles for *rac*-**7**, *meso*-**7**, *rac*-**3**, *rac*-**8**, and *rac*-**9** determined by DFT with the corresponding values from the X-ray structures. The calculated Zr−N bond lengths agree with the X-ray values to within an average of 0.02

(9) For RFF dynamics calculations on all zirconocenes containing a chelated bis-amide ligand, an explicit constraint term for the N−Zr−N angle was incorporated into the RFF parameter file. This term constrained the N−Zr−N angle to 88° with a force constant of 1000. The same constraint was used for all chelated bis-amide complexes. Addition of this constraint term provided an improved starting structure for all DFT optimizations. This constraint was not applied to zirconocenes containing monodentate amide ligands since RFF was able to accurately reproduce the N−Zr−N angle in these cases. This constraint was not applied to the subsequent DFT calculations.

(10) (a) Becke, A. D. *Phys. Rev. A* **1988**, *38*, 3098. (b) Becke, A. D. *J. Chem. Phys*. **1993**, *98*, 1372. (c) Becke, A. D. *J. Chem. Phys*. **1993**, *98*, 5648.

(11) Lee, C.; Yang, W.; Parr, R. G. *Phys. Rev. B* **1988**, *37*, 785.

(12) (a) Hay, P. J.; Wadt, W. R. *J. Chem. Phys*. **1985**, *82*, 284. (b) Hay, P. J.; Wadt, W. R. *J. Chem. Phys*. **1985**, *82*, 299.

(13) Frisch, M. J.; Trucks, G. W.; Schlegel, H. B.; Scuseria, G. E.; Robb, M. A.; Cheeseman, J. R.; Zakrzewski, V. G.; Montgomery, J. A., Jr.; Stratmann, R. E.; Burant, J. C.; Dapprich, S.; Millam, J. M.; Daniels, A. D.; Kudin, K. N.; Strain, M. C.; Farkas, O.; Tomasi, J.; Barone, V.; Cossi, M.; Cammi, R.; Mennucci, B.; Pomelli, C.; Adamo, C.; Clifford, S.; Ochterski, J.; Petersson, G. A.; Ayala, P. Y.; Cui, Q.; Morokuma, K.; Malick, D. K.; Rabuck, A. D.; Raghavachari, K.; Foresman, J. B.; Cioslowski, J.; Ortiz, J. V.; Stefanov, B. B.; Liu, G.; Liashenko, A.; Piskorz, P.; Komaromi, I.; Gomperts, R.; Martin, R. L.; Fox, D. J.; Keith, T.; Al-Laham, M. A.; Peng, C. Y.; Nanayakkara, A.; Gonzalez, C.; Challacombe, M.; Gill, P. M. W.; Johnson, B. G.; Chen, W.; Wong, M. W.; Andres, J. L.; Head-Gordon, M.; Replogle, E. S.; Pople, J. A. *Gaussian 98*, revision A.11.2; Gaussian, Inc.: Pittsburgh, PA, 1998.

(14) Dunning, T. H.; Hay, P. J. In *Modern Theoretical Chemistry*; Schaefer, H. F., III, Ed.; Plenum: New York, 1976; Vol. 3, p 1.

(15) The frequency analysis required to obtain these values requires that the structure be at a stationary point for the specified level of theory. Thus, a geometry optimization at LANL2DZ would be necessary to obtain these values.

(16) LoCoco, M. D.; Jordan, R. F. *Abstracts of Papers*, 225th ACS National Meeting, New Orleans, LA, United States, March 23−27, 2003, INOR-723.

(17) Christopher, J. N.; Diamond, G. M.; Jordan, R. F.; Petersen, J. L. *Organometallics* **1996**, *15*, 4038.

(18) Diamond, G. M.; Jordan, R. F.; Petersen, J. L. *J. Am. Chem. Soc*. **1996**, *118*, 8024.

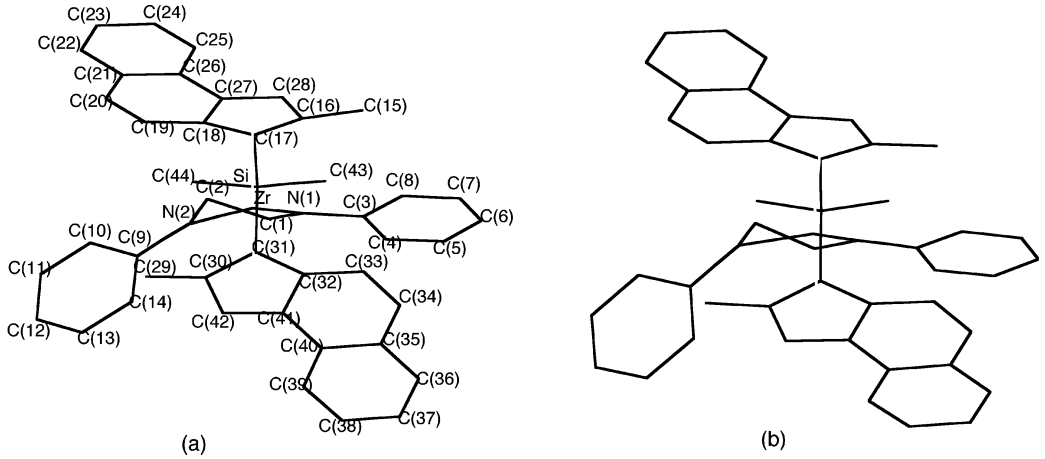

Figure 2. (a) Calculated (B3LYP/LANL2MB) structure for *rac*-(MBSBI)Zr{PhN$(CH_2)_2$NPh} (*rac*-**7**). H atoms are omitted. Bond distances (Å): Zr−N(1) 2.11, Zr−N(2) 2.06, Zr−Centroid(1) 2.42, Zr−Centroid(2) 2.36. Bond angles (deg): N(1)−Zr−N(2) 82.5, Centroid(1)−Zr−Centroid(2) 118.8. Torsion angles (deg): N(2)−Zr−N(1)−C(3) 168.6, C(9)−N(2)−Zr−N(1) −140.9. ∑ angles around N (deg): N(1) 359.8, N(2) 359.5. (b) X-ray structure of *rac*-**7**.[2a]

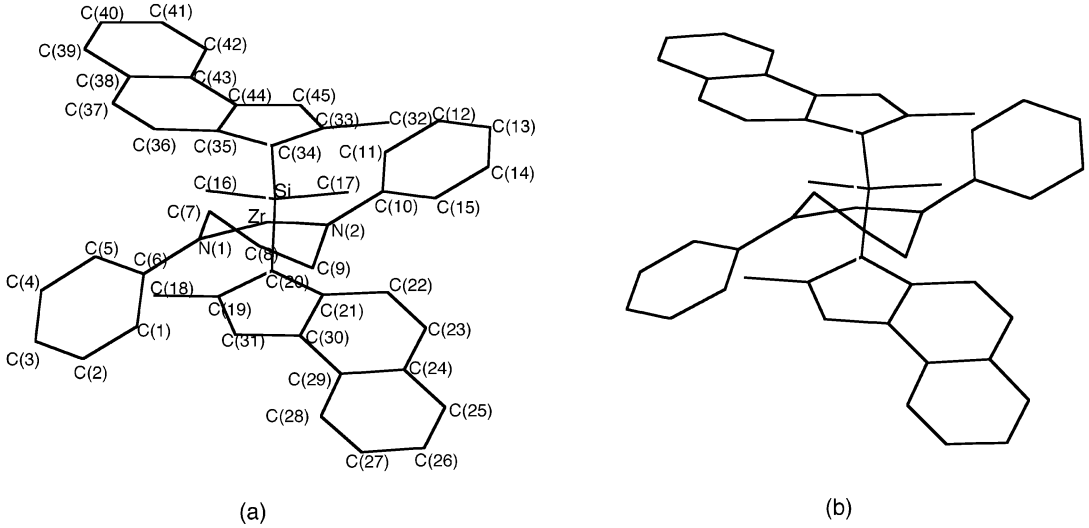

Figure 3. (a) Calculated (B3LYP/LANL2MB) structure for *rac*-(MBSBI)Zr{PhN$(CH_2)_3$NPh} (*rac*-**3**). H atoms are omitted. Bond distances (Å): Zr−N(1) 2.07, Zr−N(2) 2.07, Zr−Centroid(1) 2.39, Zr−Centroid(2) 2.39. Bond angles (deg): N(1)−Zr−N(2) 87.4, Centroid(1)−Zr−Centroid(2) 118.9. Torsion angles (deg): N(2)−Zr−N(1)−C(6) −143.2, C(10)−N(2)−Zr−N(1) 143.1. ∑ angles at N (deg): N(1) 359.9, N(2) 359.9. (b) X-ray structure of *rac*-**3**.[2a]

Table 1. Deviations of Ring Atoms from the N−Zr−N Plane for *meso*-7, *rac*-7, and *rac*-3

	DFT, Å	X-ray, Å
meso-**7**		
C(9)	−0.29	−0.318
C(2)	0.17	0.122
C(1)	0.74	0.737
C(3)	−0.61	−0.876
rac-**7**		
C(9)	−0.60	−0.831
C(2)	0.72	0.929
C(1)	0.13	0.024
C(3)	−0.20	−0.198
rac-**3**		
C(6)	−0.64	−0.719
C(7)	0.75	0.852
C(8)	0.00	0.116
C(9)	−0.76	−0.667
C(10)	0.70	0.639

Å (1.00%). The largest deviation in Zr−N bond length is 0.05 Å. However, the calculated Zr−Centroid and Zr−$C_{indenyl}$ distances are an average of 0.08 Å (3.46% for Zr−Centroid) longer than the X-ray values. The largest deviation in Zr−Centroid bond length is −0.11 Å. The largest deviations between calculated and X-ray bond angles range from 3.5° (3.5%) for N−Zr−N to 4.0° (3.2%) for Centroid−Zr−Centroid.

The fact that the B3LYP/LANL2MB geometry optimizations overestimate the Zr−Centroid bond distance by an average of 0.08 Å is consistent with previous computational studies of metallocenes and can be attributed to the use of the minimal basis set and the effective core potential in LANL2MB. Swart and Snijders[19] investigated the influence of basis set and DFT potentials on the calculated geometries of simple first-row metallocenes. This study evaluated a range of DFT exchange−correlation potentials combined with a frozen core basis for the metals. Use of a minimal basis set to describe carbon and hydrogen atoms resulted in an average deviation for the M−Centroid distance of +0.0736 Å. The addition of split valence and polarization functions to the basis set improved the average deviation to +0.0278 Å. Cook[20] reports that a BLYP/

(19) Swart, M.; Snijders, J. G. *Theor. Chem. Acc.* **2003**, *110*, 34.

Table 2. Comparison of Metallocene Geometries Calculated by DFT (B3LYP/LANL2MB) and Determined by X-ray Diffraction

parameter	DFT[a]	X-ray[b]	deviation (X-ray-DFT)[c]	% deviation[d]	parameter	DFT[a]	X-ray[b]	deviation (X-ray-DFT)[c]	% deviation[d]
Zr−N, Å					Si−indenyl, Å				
rac-**7**	2.11	2.15	0.04	1.86	*rac*-**7**	1.94	1.87	−0.07	3.74
	2.06	2.07	0.01	0.48		1.94	1.88	−0.06	3.19
meso-**7**	2.06	2.10	0.04	1.90	*meso*-**7**	1.94	1.87	−0.06	3.21
	2.10	2.14	0.04	1.90		1.95	1.88	−0.07	3.72
rac-**3**	2.07	2.07	0	0	*rac*-**3**	1.95	1.88	−0.07	3.72
	2.07	2.12	0.05	2.36		1.95	1.87	−0.08	4.28
rac-**8**	2.07	2.07	0	0	*rac*-**8**	1.93	1.86	−0.07	3.76
	2.07	2.07	0	0		1.93	1.86	−0.07	3.76
rac-**9**	2.07	2.06	−0.01	0.49	*rac*-**9**				
	2.07	2.05	−0.02	0.96	average absolute[e]	1.94	1.87	−0.07	3.67
average absolute[e]	2.08	2.10	0.02	1.00	N−Zr−N, deg				
Zr−Centroid, Å					*rac*-**7**	82.5	81.3	−1.2	1.48
rac-**7**	2.36	2.27	−0.09	3.96	*meso*-**7**	82.9	81.4	−1.5	1.84
	2.42	2.34	−0.08	3.41	*rac*-**3**	87.4	86.7	−0.7	0.81
meso-**7**	2.46	2.35	−0.11	4.68	*rac*-**8**	96.4	97.0	0.6	0.62
	2.35	2.27	−0.08	3.52	*rac*-**9**	95.9	99.4	3.5	3.52
rac-**3**	2.39	2.29	−0.10	4.37	average absolute[e]	89.1	89.6	1.5	1.65
	2.39	2.34	−0.05	2.14	Cent−Zr−Cent, deg				
rac-**8**	2.40	2.32	−0.08	3.45	*rac*-**7**	118.8	122.8	4.0	3.26
	2.40	2.32	−0.08	3.45	*meso*-**7**	119.4	122.6	3.2	2.61
rac-**9**	2.38	2.31	−0.07	3.03	*rac*-**3**	119.0	123.0	4.0	3.25
	2.38	2.32	−0.06	2.59	*rac*-**8**	119.6	122.9	3.3	2.69
average absolute[e]	2.39	2.30	0.08	3.46	*rac*-**9**	120.7	122.2	1.5	1.23
Average Zr−$C_{indenyl}$, Å					average absolute[e]	120.6	123.3	3.2	2.61
rac-**7**	2.69	2.60	−0.09	3.46	Ind−Si−Ind, deg				
meso-**7**	2.70	2.61	−0.09	3.81	*rac*-**7**	81.0	82.2	1.2	1.46
rac-**3**	2.64	2.57	−0.07	2.72	*meso*-**7**	81.8	82.2	0.04	0.05
rac-**8**	2.70	2.62	−0.08	3.05	*rac*-**3**	81.2	82.7	1.5	1.81
rac-**9**	2.68	2.60	−0.08	3.07	*rac*-**8**	82.2	83.2	1.0	1.20
average absolute[e]	2.68	2.59	0.08	3.22	*rac*-**9**				
N−R,[f] Å					average absolute[e]	81.3	82.4	1.0	1.3
rac-**7**	1.46	1.41	−0.05	3.55	∑(angles at N), deg				
	1.47	1.43	−0.04	2.80	*rac*-**7**	359.8	359.3	−0.5	0.14
meso-**7**	1.47	1.42	−0.05	3.52		359.5	354.4	−5.1	1.43
	1.46	1.40	−0.06	4.29	*meso*-**7**	351.3	344.4	−6.9	0.02
rac-**3**	1.48	1.44	−0.04	2.78		360.2	359.4	−0.8	0.22
	1.48	1.41	−0.07	4.96	*rac*-**3**	359.9	359.4	−0.5	0.14
rac-**8**	1.52	1.46	−0.06	4.11		359.9	359.5	−0.4	0.11
	1.51	1.45	−0.06	4.14	*rac*-**8**	359.5	359.6	0.1	0.03
	1.52	1.46	−0.06	4.11		359.5	359.6	0.1	0.03
	1.51	1.45	−0.06	4.14	*rac*-**9**	359.6	359.5	−0.1	0.03
rac-**9**	1.51	1.45	−0.06	4.14		359.6	359.3	−0.3	0.08
	1.52	1.48	−0.04	2.70	average absolute[e]	358.9	357.4	1.5	0.22
	1.51	1.47	−0.04	2.72					
	1.52	1.45	−0.07	4.83					
average absolute[e]	1.49	1.43	0.06	3.77					

[a] Values for the given parameter calculated by DFT for *rac*-**7**, *meso*-**7**, *rac*-**3**, *rac*-**8**, and *rac*-**9**. [b] Values for the given parameter determined by X-ray diffraction for *rac*-**7**, *meso*-**7**, *rac*-**3**, *rac*-**8**, and *rac*-**9**. [c] (crystallographic − calculated). Negative values indicate overestimation by the calculated value vs X-ray. [d] [(crystallographic − calculated)/(crystallographic)] × 100%. [e] Absolute average % deviation = [{∑(|crystallographic − calculated|)/(crystallographic)}/(occurrences)]. [f] Values for both N−*Ph* bond distances in *rac*-**7**, *meso*-**7**, and *rac*-**3**. Values for all four N−C bond distances in *rac*-**8** and *rac*-**9**.

LANL1MB[11,21] optimization of ferrocene resulted in an Fe−Centroid deviation of +0.1637 Å. As in our study, the minimal basis set with the Hay and Wadt effective core potential was found to overestimate the M−Centroid distance. The effect of the Hay and Wadt effective core potential combined with a double-ξ split valence basis on the metal was addressed by Linnolahti et al.[22] in their study of bridged zirconocene dichlorides. An optimization at B3LYP/LANL2DZ resulted in a Zr−Centroid deviation of 0.074 Å for (EBI)$ZrCl_2$, whereas a B3LYP/6-311G** optimization of (EBI)$ZrCl_2$ resulted in a Zr−Centroid deviation of only 0.032 Å. We performed a B3LYP/LANL2DZ geometry optimization of *rac*-**8** and found a Zr−Centroid deviation of 0.13 Å (vs 0.08 Å at LANL2MB). Thus, the Zr−Centroid distance in simple zirconocenes is overestimated even when the Hay and Wadt effective core potential is combined with a double-ξ basis on the metal and first-row atoms.

Trend in Zr−$C_{indenyl}$ Bond Lengths. Bis-indenyl zirconocenes can exhibit slip distortions toward η^3-coordination.[23] The degree of slippage may be quantified by the "slip parameter" Δ_{av}(M−C), which is defined as the difference between the average of the M−C(8) and M−C(9) distances and the average of the M−C(1), M−C(2), and M−C(3) distances, using the atom-numbering scheme in Figure 4.[24]

(20) Cook, D. *Int. J. Quantum Chem.* **1995**, *53*, 309.
(21) Hay, P. J.; Wadt, W. R. *J. Chem. Phys.* **1985**, *82*, 270.
(22) Linnolahti, M.; Hirva, P.; Pakkanen, T. A. *J. Comput. Chem.* **2001**, *22*, 51.
(23) Christopher, J. N.; Jordan, R. F.; Petersen, J. L.; Young, V. G., Jr. *Organometallics* **1997**, *16*, 3044, and references therein.
(24) Faller, J. W.; Crabtree, R. H.; Habib, A. *Organometallics* **1985**, *4*, 929.

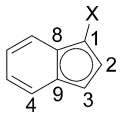

Figure 4. Atom-numbering scheme for the determination of the slip parameter Δ_{av}(M−C).

Table 3. Comparison of Δ_{av}(M−C) Values Determined by DFT and X-ray Diffraction for Selected Zirconocene Amide Complexes

	Δ_{av}(M−C), Å	
	DFT	X-ray
meso-**7**	−0.040	−0.031
	0.212	0.162
rac-**7**	−0.050	0.016
	−0.034	−0.009
rac-**3**	−0.027	0.072
	−0.027	0.070
rac-**8**	0.062	0.109
	0.063	0.110
rac-**9**	0.067	0.099
	0.067	0.121

Table 4. Angle between the Planes of the Six-Membered and Five-Membered Indenyl Rings (C6−C5 Angle) for DFT and X-ray Structures

	C6−C5 angle, deg		X-ray − DFT, deg
	DFT	X-ray	
meso-**7**	10.8	9.6	−1.2
	10.2	7.1	−3.1
rac-**7**	9.7	6.3	−3.4
	9.8	6.6	−3.2
rac-**3**	9.6	10.4	0.8
	9.6	4.7	−4.9
rac-**8**	7.4	2.8	−4.6
	7.3	2.8	−4.7
rac-**9**	7.8	2.6	−5.2
	7.8	3.3	−4.5

As summarized in Table 3, the DFT structures reproduce important trends in Zr−$C_{indenyl}$ bond lengths. In cases where the X-ray structure contains a slipped indenyl ring with Δ_{av}(M−C) ≥ 0.1 Å, the corresponding calculated Δ_{av}(M−C) value is greater than 0.06 Å. In cases where the X-ray structure contains an indenyl ring that is not strongly slipped, the calculated Δ_{av}(M−C) value is in the range −0.03 to −0.05 Å. In particular, the DFT calculation correctly predicts that *meso*-**7** has one strongly slipped indenyl ligand.

Deviation of the C6 Ring from the Plane of the C5 Ring. Another common distortion of an indenyl ligand is bending of the six-membered ring out the plane of the five-membered ring. Table 4 lists the angles between the planes of the six-membered and five-membered indenyl rings (C6−C5 angle) for the DFT and X-ray structures. The DFT calculation consistently overestimates the C6−C5 angle by 1−5°.

Validation of Methodology: Energies. The ability of the DFT method to predict the relative energies of *rac* and *meso ansa*-zirconocene amide complexes was explored by comparison of *rac*/*meso* ratios predicted by DFT with experimentally measured thermodynamic *rac*/*meso* ratios. In favorable cases, *rac*- and *meso*-(XBI)-$Zr(NR_2)_2$ complexes can be equilibrated by reversible amine elimination reactions in the presence of NR_2H, as illustrated for the specific case of **9** in Scheme 4, which enables experimental determination of the thermodynamic *rac*/*meso* ratio.[18,23,25,26] Calculated and

Scheme 4

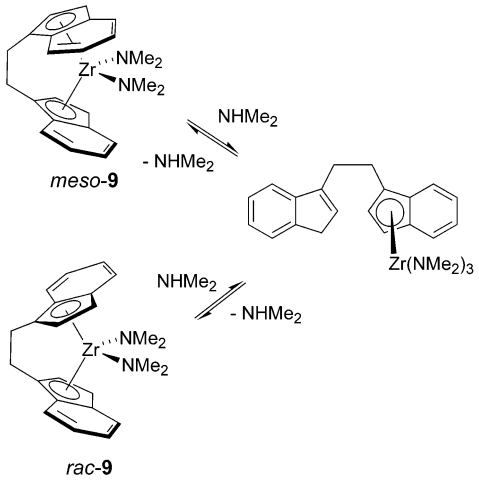

Table 5. Experimentally Determined and Calculated (B3LYP/LANL2DZ//B3LYP/LANL2MB) Thermodynamic *Rac*/*Meso* Ratios and Corresponding Differences in *rac* and *meso* Energies ($\Delta E_{rac-meso}$) for *ansa*-Zirconocene Amide Complexes

		experimental		DFT	
zirconocene	*T*, °C	*rac*/*meso* ratio	$\Delta E_{rac-meso}$,[a] kcal/mol	*rac*/*meso* ratio[b]	$\Delta E_{rac-meso}$,[c] kcal/mol
8	23	4:1	−0.8	1.4:1	−0.2
(EBI)Zr-(pyrrolidide)$_2$	100	7:1	−1.4	7.6:1	−1.5
9	23	>45:1	−2.2	6.1:1	−1.1
10	23	1:2	+0.4	1:9.4	+1.3

[a] Value for $E_{rac} - E_{meso}$ at the experimental temperature assuming a Boltzmann distribution based on the experimental *rac*/*meso* ratio. [b] Calculated for the experimental temperature from a Boltzmann distribution of B3LYP/LANL2DZ energies for *rac* and *meso* diastereomers. [c] Calculated value for $E_{rac} - E_{meso}$ from B3LYP/LANL2DZ energies. Thermodynamic corrections to total energy are not included since the frequency calculation was performed using LANL2MB.

experimental *rac*/*meso* ratios and corresponding differences in *rac* and *meso* energies ($\Delta E_{rac-meso}$) for several (XBI)$Zr(NR_2)_2$ complexes are compared in Table 5.

The data in Table 5 indicate that the B3LYP/LANL2DZ//B3LYP/LANL2MB calculation reproduces the general trend in the relative energies of the *rac* and *meso* isomers. The *rac* isomer was correctly predicted to be favored for **8** and **9**, whereas the *meso* isomer was correctly predicted to be favored for $Me_2Si(3\text{-}^tBuC_5H_3)_2$-$Zr(NMe_2)_2$ (**10**). The experimental trend was not reproduced by the lower level B3LYP/LANL2MB energies or simple RFF energies.

Energies of *rac* and *meso ansa*-Zirconocenes that Contain Chelated Bis-amide Ligands. The studies described above provide a reasonably efficient and accurate method for calculating the structures and relative energies of *rac* and *meso ansa*-zirconocene amide complexes. Using this approach, we investigated the (MBSBI)Zr system in detail to probe the origin of stereoselectivity in chelate-controlled metallocene syntheses. The calculated energy difference between the *rac*

(25) Diamond, G. M.; Jordan, R. F.; Petersen, J. L. *Organometallics* **1996**, *15*, 4030.
(26) Diamond, G. M.; Jordan, R. F.; Petersen, J. L. *Organometallics* **1996**, *15*, 4045.

Table 6. Calculated (B3LYP/LANL2DZ//B3LYP/LANL2MB) Energy Differences and Corresponding Calculated Thermodynamic *rac*/*meso* Ratios, and Experimental *rac*/*meso* Product Ratios from Chelate-Controlled Syntheses, for 3, 7, and 11

	DFT		experimental
	$\Delta E_{rac-meso}$,[a] kcal/mol	predicted thermodynamic *rac*/*meso* ratio[b]	*rac*/*meso* product ratio
3	−5.7	100% *rac* (23 °C)	100% *rac*[c] (23 °C)
7	−2.4	59:1 (5 °C)	2:1[d] (5 °C)
11	−0.4	2:1 (0 °C)	100% *meso*[e] (0 °C)

[a] Calculated value for $E_{rac} - E_{meso}$. [b] From a Boltzmann distribution of B3LYP/LANL2DZ energies for *rac* and *meso* diastereomers. [c] Product ratio from Scheme 1. [d] Product ratio from Scheme 3. [e] Product ratio from Scheme 5.

and *meso* diastereomers ($\Delta E_{rac-meso}$) and the corresponding estimated thermodynamic *rac*/*meso* ratios for **3** and **7** are given in Table 6. These data show that the *rac* isomer is more strongly favored over the *meso* isomer for **3** than for **7**. Table 6 also lists the observed product ratios for **3** and **7** from the chelate-controlled syntheses in Schemes 1 and 3. It is interesting to note that for these cases the trend in observed *rac*/*meso* product ratios parallels the trend in calculated thermodynamic *rac*/*meso* ratios.

Structure of *meso*-(MBSBI)Zr{PhN(CH$_2$)$_3$NPh} (*meso*-3). We analyzed the structure of *meso*-**3** in detail to probe why this experimentally unobserved species is so much less stable than the *rac* isomer. The calculated structure of *meso*-**3** is shown in Figure 5. The Zr{PhN(CH$_2$)$_3$NPh} ring has a twist conformation that places the C(1)−C(6) N-*Ph* group in a sterically congested environment close to the C(19)−C(31) benzindenyl ligand. *meso*-**3** exhibits several subtle structural differences compared to *rac*-**3**, which likely arise from the unfavorable steric interactions between these groups. First, the C(19)−C(31) benzindenyl ligand is strongly η^3-slip distorted (Δ_{av}(M−C) = 0.188 Å), while the other benzindenyl ligand is not (Δ_{av}(M−C) = −0.028 Å). Second, the C6−C5 plane angle for the slip-distorted benzindenyl group is 14.2°, which is outside of the range calculated or observed for similar structures (Table 4). The nonslipped indenyl has a C6−C5 angle of 10.4°, which is at the large end of the range for the metallocenes in Table 4. Third, the Zr{PhN(CH$_2$)$_3$NPh} ring is slightly flattened on the congested side of the metallocene, compared to that in *rac*-**3**. The degree of flattening of the ring can be assessed from the deviations of the chelate ring atoms from the N−Zr−N plane, which for the calculated structure of *meso*-**3** and the calculated and X-ray structures of *rac*-**3** are given in Table 7. The sum of the displacements of C(6) and C(7) from the N−Zr−N plane is lower for *meso*-**3** (1.13 Å) than for the calculated or X-ray structures of *rac*-**3** (1.39 and 1.57 Å), which indicates that the C(6)−C(7) side of the Zr{PhN(CH$_2$)$_3$NPh} ring is flatter in the former compound than in the latter.

The closest atom−atom contacts in *meso*-**3** are listed in Figure 6. The closest carbon−carbon contact is between the N-*Ph* ipso carbon C(6) and the indenyl ring carbon C(29). Close contacts between the N-*Ph* ortho hydrogen (H(58)) and the C(33)−C(45) indenyl ligand are also present. The equatorial hydrogen of the C(7) methylene group (H(92)) makes close contact with the C(1)−C(6) N-*Ph* ring, which pushes this ring closer to

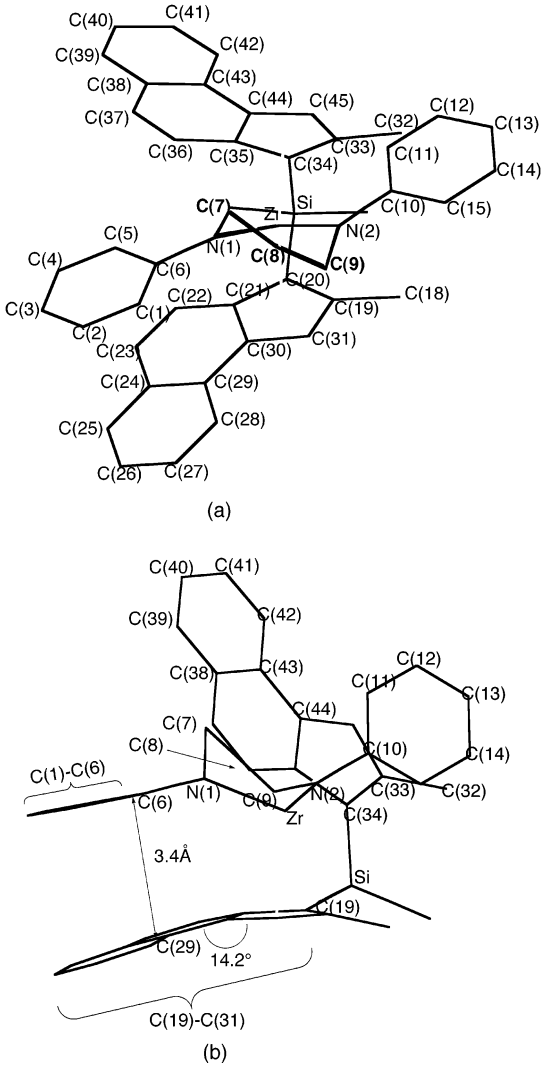

Figure 5. Calculated structure of *meso*-(MBSBI)Zr{PhN(CH$_2$)$_3$NPh} (*meso*-**3**). (a) Front view. (b) Alternate view highlighting the exaggerated C6−C5 angle in the C(19)−C(31) benzindenyl group. Bond distances (Å): Zr−N(1) 2.08, Zr−N(2) 2.07, Zr−Centroid(1) 2.38, Zr−Centroid(2) 2.43. Bond angles (deg): N(1)−Zr−N(2) 88.1, Centroid(1)−Zr−Centroid(2) 119.1. Torsion angles (deg): N(2)−Zr−N(1)−C(6) −153.2, C(10)−N(2)−Zr−N(1) 136.4. Σ angles at N (deg): N(1) 360.0, N(2) 359.9

Table 7. Distance of Key Atoms from the N−Zr−N Plane for *rac*-3 and *meso*-3

	rac-**3**		*meso*-**3**
	X-ray	DFT	DFT
C(6)	−0.719	−0.64	−0.48
C(7)	0.852	0.75	0.65
C(8)	0.116	0.00	0.20
C(9)	−0.667	−0.76	−0.88
C(10)	0.639	0.70	0.70
|C(6)| + |C(7)|[a]	1.57	1.39	1.13
|C(9)| + |C(10)|[b]	1.31	1.46	1.58

[a] Distance across N−Zr−N plane measured from C(6) to C(7). [b] Distance across N−Zr−N plane measured from C(9) to C(10).

the C(19)−C(31) benzindenyl ligand than to the C(33)−C(45) benzindenyl ligand. The crowding in *meso*-**3** would be exacerbated if the η^3-slip and C6−C5 angle distortions of the C(19)−C(31) benzindenyl ligand or the flattening of the Zr{PhN(CH$_2$)$_3$NPh} ring were relaxed.

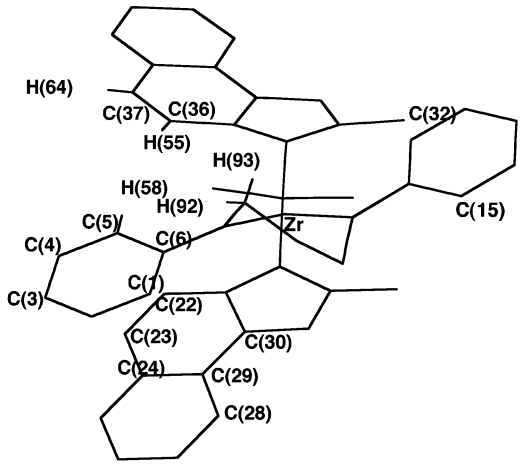

Closest Contacts

C(6)-C(29)	3.4Å	H(58)-H(55)	3.0Å
C(6)-C(24)	3.6Å	H(58)-H(64)	2.9Å
C(6)-C(30)	3.5Å	H(58)-C(36)	2.6Å
C(1)-C(29)	3.5Å	H(58)-C(37)	2.9Å
C(1)-C(28)	3.6Å	H(92)-C(6)	2.4Å
C(5)-C(24)	3.5Å		
C(5)-C(23)	3.4Å		
C(5)-C(22)	3.5Å		
C(3)-C(25)	3.6Å		
C(4)-C(24)	3.6Å		
C(4)-C(23)	3.5Å		
C(32)-C(15)	3.5Å		

Figure 6. Closest contacts in *meso*-**3**. Only those H atoms that are involved in close contacts are shown.

These results show that an η^3-slip distortion and an exaggerated C6−C5 plane angle in the C(19)−C(31) benzindenyl ring and a subtle flattening of the Zr{PhN-$(CH_2)_3$NPh} chelate ring occur in *meso*-**3**. These features alleviate steric crowding between the C(1)−C(6) N-*Ph* group and the C(19)−C(31) benzindenyl ligand on the crowded side of the metallocene. Although the slip distortion also occurs in other *ansa*-zirconocene amide complexes, the combination of these features appears to be unique to *meso*-**3** and likely destabilizes this species relative to the *rac* isomer.

Table 9. Relative Energies of Local Minima for *rac*-3, *meso*-3, and 5

confor-mation	*E* of *rac*-**3** vs *rac*-**3**-twist, kcal/mol	*E* of *meso*-**3** vs *meso*-**3**-twist, kcal/mol	*E* of *meso*-**3** vs *rac*-**3**-twist, kcal/mol	*E* of **5** vs **5**-twist, kcal/mol
twist	0.0	0.0	5.7	0.0
chair	4.2	0.8	6.5	2.7
boat	6.1	1.9	7.6	3.6
envelope	4.2	2.0	7.7	

Conformational Analysis of Zr{PhN$(CH_2)_3$NPh} Complexes. A key aspect of the stereocontrol model in Scheme 2 is the hypothesis that the preferred conformation of the Zr{PhN$(CH_2)_3$NPh} chelate ring is the twist conformation. To probe this issue, a detailed conformational analysis of the Zr{PhN$(CH_2)_3$NPh} rings in *rac*-**3**, *meso*-**3**, and Cp_2Zr{PhN$(CH_2)_3$NPh} (**5**) was performed. A Zr{PhN$(CH_2)_3$NPh} ring can assume several limiting conformations, which can be defined by the displacements of the ring atoms from the N−Zr−N plane as shown in Table 8.

The twist conformation is calculated to be the global minimum for *rac*-**3**, *meso*-**3**, and **5**, which is consistent with X-ray results for *rac*-**3** and **5**.[2a,16] Local minima were also located for the boat, chair, and envelope conformations of *rac*-**3** and *meso*-**3** and for the boat and chair conformations of **5**. The energies of these species relative to their respective ground state twist conformers are listed in Table 9. The relative energies of the conformers of **5** provide an estimate of the preference for the twist conformation in the absence of steric interactions and/or structural distortions that may occur in more crowded metallocenes. The twist conformer of

Table 8. Displacement of Atoms from the N−Zr−N Plane in Limiting Conformations of Zr{PhN$(CH_2)_3$NPh} Chelate Rings[a]

Conformation	**Ph**-N	CH_2—	CH_2—	CH_2—	N-**Ph**
twist	+	-	0	+	-
boat	+	-	- -	-	+
chair	+	-	-	-	+
envelope	0	0	0	+	-

[a] + = above, 0 = in, − = below, − − = further below, the N−Zr−N plane.

Table 10. Calculated Δ_{av}(M−C) Values and C6−C5 Plane Angles for Conformers of *rac*-3 and *meso*-3

	Δ_{av}(M−C), Å	slip distorted?	C6−C5 plane angle
rac-**3**			
twist	−0.027	no	9.6
	−0.027	no	9.6
chair	0.129	yes	15.1
	0.237	yes	8.4
boat	0.100	yes	14.0
	0.156	yes	9.7
envelope	0.129	yes	15.1
	0.237	yes	8.4
meso-**3**			
twist	−0.028	no	14.3
	0.180	yes	10.5
chair	0.088	slightly	15.2
	0.205	yes	9.0
boat	0.036	no	13.8
	0.216	yes	10.8
envelope	0.041	no	13.9
	0.197	yes	11.1

5 is calculated to be 2.7 kcal/mol more stable than the chair conformer.

Table 10 lists calculated Δ_{av}(M−C) values and C6−C5 plane angles for each conformer of *rac*-**3** and *meso*-**3**. These data indicate that the chair, boat, and envelope conformers of *rac*-**3**, and all of the conformers of *meso*-**3**, contain at least one η^3-slip distorted indenyl ring. The distortions clearly work to offset bad steric interactions between the C4 carbons of the benzindenyl ligands (see numbering scheme in Figure 4) and the *ipso* carbon of the proximate N-*Ph* group. The twist conformer of *rac*-**3** is the only conformer that does not feature a significant slip distortion and is the global minimum in this system.

The energy difference between the chair and twist conformers of *rac*-**3** ($\Delta E_{chair-twist}$ = 4.2 kcal/mol) is 1.5 kcal/mol greater than the corresponding energy difference for **5**. Thus, steric interactions between the benzindenyl and $[PhN(CH_2)_3NPh]^{2-}$ ligands as well as the η^3-slip and C6−C5 angle distortions in the chair conformer of *rac*-**3** can be estimated to destabilize the chair by about 1.5 kcal/mol. In contrast, for *meso*-**3**, the twist conformer is only 0.8 kcal/mol more stable than the chair. In this case the η^3-slip distortion and exaggerated C6−C5 angle in one of the benzindenyl groups and the flattening of the Zr{PhN$(CH_2)_3$NPh} ring destabilize the ground state twist conformer.

Prediction of *rac/meso* Selectivity. As noted above, the trend in *rac*/*meso* ratios obtained in the syntheses of **3** (Scheme 1, 100% *rac*) and **7** (Scheme 3, *rac/meso* = 2:1) *qualitatively* parallels the trend in calculated $\Delta E_{rac-meso}$ values (**3**: −5.7 kcal/mol; **7**: −2.4 kcal/mol). This result suggests that calculated product $\Delta E_{rac-meso}$ values may provide a predictive guide for stereoselective metallocene synthesis. To test the possibility, we modeled and explored the synthesis of a bis-cyclopentadienyl zirconocene, $Me_2Si(3\text{-}^tBu\text{-}C_5H_3)_2$Zr{PhN$(CH_2)_3$NPh} (**11**). As shown in Table 6, the B3LYP/LANL2DZ//B3LYP/LANL2MB calculated $\Delta E_{rac-meso}$ for **11** is −0.40 kcal/mol, which is the smallest $\Delta E_{rac-meso}$ value that we have calculated for an *ansa*-zirconocene containing a chelated bis-amide ligand. Assuming that the relative energies of the stereodetermining transition states that lead to *rac*- and *meso*-**11** will track the relative product energies, this result suggests that the preference for formation of *rac*-**11** should be much less for this compound than for the other metallocenes that were modeled above (Table 6). Consistent with this prediction, Jordan et al. found that *only meso*-**11** is formed in the reaction of **1** and $Li_2[Me_2Si(3\text{-}^tBu\text{-}C_5H_3)_2]$ (Scheme 5).[2b] A discussion of the stereocontrol mechanism in this system is presented elsewhere.[2b]

Scheme 5

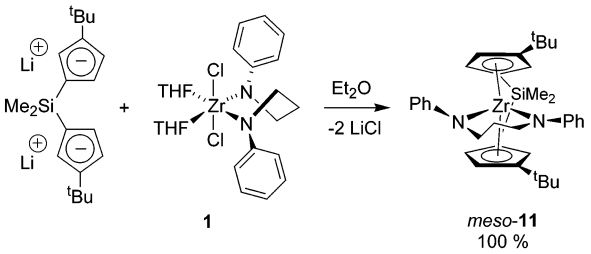

Discussion

An efficient DFT computational protocol to predict the structures and relative energies of zirconocene amide complexes has been implemented, which involves the following steps. (i) Starting points for the DFT calculation are obtained by conducting a molecular mechanics conformational search using the RFF force field. This search is necessary for zirconocenes containing chelated bis-amide ligands, since stationary points containing several chelate ring conformations were observed in these cases. (ii) The RFF geometry can be refined with DFT using the B3LYP functional and the LANL2MB basis set. (iii) Relative energies of the *rac* and *meso* diastereomers of *ansa*-zirconocene amides ($\Delta E_{rac-meso}$) are obtained by LANL2DZ single-point energy calculations on the LANL2MB geometries. Experimental relative energies were not accurately reproduced with the LANL2MB basis set. Using this method, X-ray crystal structures and experimental trends in $\Delta E_{rac-meso}$ values for a series of zirconocenes with terminal and chelated bis-amide ligands were reproduced with reasonable accuracy. This procedure was used to study the structures and relative energies of zirconocene bis-amides to probe the origins of stereoselectivity in chelate-controlled zirconocene syntheses.

In the absence of overriding steric interactions, the most stable conformation of Zr{PhN$(CH_2)_3$NPh} rings in zirconocenes is the twist conformation. For Cp_2Zr-{PhN$(CH_2)_3$NPh} (**5**), the twist conformer is 2.7 kcal/mol more stable than the chair and 3.6 kcal/mol more stable than the boat. Adding substituents to the Cp rings can influence the relative stabilities of the Zr{PhN$(CH_2)_3$NPh} ring conformations by introducing unfavorable steric interactions between the Zr{PhN-$(CH_2)_3$NPh} ring and the substituted Cp ligands, but, in general, the preference for the twist conformation is maintained.

rac-(MBSBI)Zr{PhN$(CH_2)_3$NPh} (*rac*-**3**) is 5.7 kcal/mol more stable than the *meso* isomer because the latter species must undergo a combination of distortions to accommodate the favored twist conformation of the Zr{PhN$(CH_2)_3$NPh} ring, due to steric interactions between the N-*Ph* and benzindenyl groups on the crowded side of the metallocene. These distortions include a significant η^3-slip and an exaggerated C6−C5 plane angle for one benzindenyl ligand and a

flattening of the Zr{PhN(CH_2)$_3$NPh} ring. The chair, boat, and envelope conformers of *meso*-**3** are even less stable than the twist conformer. Similar results are expected for other *ansa*-(XBI)Zr{PhN(CH_2)$_3$NPh} complexes.

In contrast, *rac*-(MBSBI)Zr{PhN(CH_2)$_2$NPh} (*rac*-**7**) is only 2.4 kcal/mol more stable than the *meso* isomer. In this case, the Zr{PhN(CH_2)$_2$NPh} ring adopts an envelope conformation in which one N-*Ph* ring lies in the N−Zr−N plane and steric interactions on the crowded side of the *meso* metallocene unit are minimized. Although one benzindenyl ring in *meso*-**7** is η^3-slipped, this distortion is not accompanied by an exaggerated C6−C5 plane angle or a distortion of the Zr{PhN(CH_2)$_2$NPh} ring conformation from that in *rac*-**7**. The calculated $\Delta E_{rac-meso}$ value for Me_2Si(3-^{t}Bu-C_5H_3)$_2$Zr{PhN(CH_2)$_3$NPh} (**11**) is only −0.40 kcal/mol.

The current working model for stereocontrol in chelate-controlled metallocene syntheses via reaction of Zr{RN(CH_2)$_n$NR}Cl_2(THF)$_2$ compounds with lithium *ansa*-bisindenyl or *ansa*-biscyclopentadienyl reagents assumes that the stereodetermining transition states for the second indenyl or cyclopentadienyl additions resemble the products and that, therefore, the steric interactions in the products are strongly expressed in these transition states. In this model, the *rac*/*meso* selectivities should vary in the same fashion as the thermodynamic *rac*/*meso* ratios of the product metallocenes. Consistent with this model, the trend in *rac*/*meso* selectivity obtained in the syntheses of **3**, **7**, and **10** qualitatively parallels the trend in calculated $\Delta E_{rac-meso}$ values for these metallocenes, as summarized in Table 6. Therefore we expect that the computational procedures described here will provide a useful and predictive aid for the design of stereoselective chelate-controlled metallocene syntheses. However, it is clear that more extensive and sophisticated experimental and computational studies, and in particular, a more detailed understanding of how chloride ligands are displaced by indenyl or cyclopentadienyl ligands, will be required to fully understand the stereocontrol mechanisms in these reactions.

Acknowledgment. We thank Dr. Anthony K. Rappé for providing the code for the RFF force field. D.C.W. thanks Lake Forest College for financial support. Work at the University of Chicago was supported by the National Science Foundation (CHE-0212210).

Supporting Information Available: Listing of Cartesian coordinates, total energies, and number of imaginary frequencies for all structures reported in Tables 1−10. This material is available free of charge via the Internet at http://pubs.acs.org.

OM049576D